Formation of complex intermetallic phases in novel refractory high-entropy alloys NbMoCrTiAl and TaMoCrTiAl: thermodynamic assessment and experimental validation

Franz Müller[a], Bronislava Gorr[a], Hans-Jürgen Christ[a], Hans Chen[b], Alexander Kauffmann[b], Stephan Laube[b] and Martin Heilmaier[b]

Affiliation

[a]Institut für Werkstofftechnik, Universität Siegen, Siegen, Germany; [b]Institut für Angewandte Materialien, Karlsruher Institut für Technologie (KIT), Karlsruhe, Germany

Abstract

In this work, we present the results of the thermodynamic assessment of two equiatomic refractory High Entropy Alloys (HEAs), namely TaMoCrTiAl and NbMoCrTiAl, in the temperature range between 700 and 1500°C. Particular attention is paid on the constitution of the intermetallic phases stable in these alloy systems. Thermodynamic calculations were performed using a self-developed thermodynamic database based on the CALPHAD (Calculation of Phase Diagram) approach. The details of the thermodynamic modelling and particular characteristics of the relevant phases within the Ta-Nb-Cr-Ti-Al system are presented. To verify the new database, the phase formation and stability of both quinary alloys in near-equilibrium conditions were studied experimentally by utilizing scanning electron microscopy (SEM) with energy dispersive spectroscopy (EDS) and electron backscatter diffraction (EBSD) as well as X-ray powder diffraction (XRD). Both equiatomic alloys reveal a complex microstructure including several intermetallic phases at intermediate temperatures. The alloy NbMoCrTiAl consists of an ordered B2 phase, $Al(Mo, Nb)_3$ and two polytypes (C14 and C15) of the Cr_2Nb Laves phase. Precipitations of Cr_2Ta Laves phase (C14, C15 and C36-type) in the B2 matrix were observed in the alloy TaMoCrTiAl. Based on the results of thermodynamic calculations, it was concluded that: (i) Nb stabilizes the $AlMo_3$ A15 phase in the alloy NbMoCrTiAl, (ii) Al and Ti play a crucial role in the formation of the ordered B2 phase in both alloys and (iii) the concentrations of Cr and/or Ta/Nb should be dramatically reduced to decrease the Laves phase volume fraction.

1. Introduction

Refractory High Entropy Alloys (RHEAs), a subgroup of HEAs, containing significant amount of refractory elements were first introduced by Senkov in 2010. RHEAs have attracted great attention in the field of high-temperature materials primarily due to their ability to maintain high strength up to 1600°C [1]. The first investigated RHEAs consisted of refractory metals Mo, Nb, Ta, V and W [1,2], later elements from Group IV (Ti, Zr and Hf), Group V (V) and Group VI (Cr) were added [3]. The intention to add Ti or Zr was that they are substantially lighter compared to the "classical" refractory metals such as W. However, these elements undergo an allotropic transformation from the low-temperature Hexagonal Close-Packed (HCP) phase to the high-temperature Body-Centered Cubic (BCC) phase. Although remarkable mechanical properties have been achieved at both, room and elevated temperatures, most of these alloys still have high densities and very low oxidation resistance. Therefore as a next step, RHEAs containing Al or Si, beside of Cr, e.g. AlNbTiV, AlCr0.5NbTiV or NbMoCrTiAl1Si have been introduced which possess lower densities than refractory HEAs (below 7 g/cm^3) [3–5] and improved oxidation resistance [3,6]. With a few exceptions, RHEAs contain intermetallic phases forming as a result of phase transformations including order-disorder transformation [7,8], spinodal decomposition [9–12], precipitation [13–15] and massive transformation [16,17]. Interestingly, some of RHEAs consisting of an A2-type matrix and B2-type precipitations resemble in appearance and properties the conventional superalloys [9,18–20].

Our previous work on derivatives within the Ta-Nb-Mo-Cr-Ti-Al system was focused on microstructural investigation, mechanical testing, and high-temperature corrosion studies. The equatomic alloys NbMoCrTiAl and TaMoCrTiAl were chosen as reference alloys for fundamental research. Experimental results show that alloys from the alloy system Ta-Nb-Mo-Cr-Ti-Al possess a promising combination of attributes such as high solidus temperature, perspective mechanical properties [21,22] and reliable oxidation resistance [6,23,24]. Alloys being developed within the alloy system mentioned above are regarded to have a high potential for high temperature applications. In our first intense microstructural investigations on the equiatomic alloy NbMoCrTiAl the results suggested an A2-type matrix and some secondary phases precipitated predominantly at the grain boundaries during cooling. Our latest works [25], however, revealed a B2-type ordered crystal structure – instead of the A2-type disordered counterpart – in several derivatives within the Ta-Nb-Mo-Cr-Ti-Al system. It was concluded that the poor ductility and high brittle-to ductile transition temperatures [22] of some of the alloys studied correlate the appearance of an ordered B2-type phase [25,26].

In general, the formation of intermetallic phases such as Laves phase (Cr_2Ta/Cr_2Nb) and A15 phase ($Al(Mo, Nb)_3$) in the Ta-Nb-Mo-Cr-Ti-Al system could be suppressed by applying sufficiently high homogenization temperatures [25]. However, the precipitation and subsequent growth of such phases at moderate temperatures – potential service temperatures – is undesired because of the typically detrimental properties of these phases, i.e. low room temperature ductility [27,28] and poor high temperature corrosion resistance [29]. To design new high temperature structural materials, which combine the most relevant properties, i.e. creep resistance, room temperature ductility and oxidation resistance, a detailed knowledge of intermetallic phases is required. In particular, the information on their exact chemical composition and the temperature range of their stability is indispensable.

Exploring the field of phase formation and stability in HEAs using exclusively experimental methods is quite complex, expensive and time-consuming. In addition, experimental studies on phase equilibria at lower temperatures, while indispensable, can last hundreds and even thousands of hours because of the very slow diffusion [30,31]. The CALPHAD approach (CALculation of PHAse Diagrams) is regarded as the most straightforward and robust method to assess the phase stability in complex alloy systems like HEAs [31,32]. This method relies on classical thermodynamics and provides information on stable or metastable equilibrium by minimizing the total Gibbs free energy. Most of the currently available thermodynamic databases have been developed for classical alloy systems that significantly differ from HEA systems as they have been established considering a single principal base element (like Ni in Ni-based or Fe in Fe-based alloys). Such databases usually do not provide reasonable results when extrapolated towards equiatomic alloys. To achieve a high quality of thermodynamic calculations for HEAs, thermodynamic databases have to be established for a system of particular interest.

The main goals of this work are (i) to give relevant information about the self-developed thermodynamic database for the TaNbMoCrTiAl system, (ii) to present and discuss the phase equilibria for two RHEAs NbMoCrTiAl and TaMoCrTiAl in the temperature range from 700 up to 1500°C, (iii) to evaluate the results of thermodynamic calculations by comparing them with corresponding results of experimental investigations and, finally (iv) to discuss the constitution of the intermetallic phases observed in the alloys studied using thermodynamic calculations and to suggest ways to reduce or even suppress the formation of such ordered phases.

2. Methodology

2.1 Materials and experimental characterization

Both alloys TaMoCrTiAl and NbMoCrTiAl were produced from elemental bulk materials by arc melting utilizing an arc-melter AM 0.5 by Edmund Bühler GmbH. It should be noted that in this paper

the nomenclature of the alloys refers to an equimolar composition; otherwise subscripts are used to designate variational element concentrations in at. %. The elements Ta, Nb, Mo, Cr, Ti and Al with purities of 99.9, 99.9, 99.96, 99, 99.98 and 99.9 %, respectively, were mixed in the required composition. The vacuum chamber of the arc melting device was pumped to a pressure of $5 \cdot 10^{-2}$ mbar and then flooded with Ar gas for three times until a high vacuum environment with $1 \cdot 10^{-4}$ mbar was established. The buttons of ~25g were melted in a water-cooled Cu crucible under working Ar pressure of ~600mbar as well as flipped and re-melted five times to ensure homogeneity of the alloying elements. After melting, the TaMoCrTiAl and NbMoCrTiAl were heat-treated at 1400 and 1300°C, respectively, both for 20h in Ar atmosphere using a tube furnace by Carbolite Gero GmbH & Co. KG and subsequently cooled in the furnace at cooling rate of 4 K/min. The chemical composition of TaMoCrTiAl was determined by ICP-OES whereas the composition of NbMoCrTiAl was analyzed using EDX. The mean chemical composition of the alloys is listed in Tab 1. The maximum deviation of the element concentration from the equimolar ratio of both alloys is equal or below 1.0 at. %.

Table 1: Chemical compositions x_i (*i* denotes the respective element) of the investigated alloys in at.%; here * denotes ICP-OES, ** indicates standard-related EDX.

alloy	**Initial heat treatment condition**	**x_i / at.%**					
		Ta	**Nb**	**Mo**	**Cr**	**Ti**	**Al**
TaMoCrTiAl*	1400°C / 20 h	20.1	–	19.5	19.8	20.4	20.2
NbMoCrTiAl**	1300°C / 20 h	–	21.0	20.5	19.1	20.1	19.3

The ingots were cut into rectangular samples into dimensions of (5x5x4) mm^3 by electrical discharge machining (EDM). The surfaces of the samples were ground after EDM to remove the as-cut surface using abrasive SiC paper up to grit P800. To study the phase stability at different temperatures, the samples were annealed in a tube furnace in Ar atmosphere at 700, 800 and 1000°C for 800, 300 and 100h, respectively, and subsequently water quenched. After the annealing treatments, the samples were again ground using SiC paper up to grit P4000 and polished using colloidal silica suspension (OPS) for final polishing. The samples were cleaned with ultrasonic in ethanol before XRD and SEM investigations. The XRD measurements were conducted on bulk specimens using an X'Pert Pro MPD diffractometer operating in Bragg-Brentano geometry with Cu-Kα radiation. Scans were carried out at 45kV and 40mA at a step size of 0.01° in 2Θ and 60s/step. For microstructure analysis, a Focused Ion Beam - Scanning Electron Microscope (FIB-SEM) DualBeam system FEI Helios Nanolab 600 was used. The FIB-SEM was equipped with additional techniques such as backscatter electron (BSE) imaging, energy-dispersive X-ray spectroscopy (EDX) as well as electron backscatter diffraction (EBSD).

2.2. Thermodynamic modeling

The details of CALPHAD methods and the models used to describe pure elements, stoichiometric compounds and solutions can be found elsewhere [33]. Here, only a brief description of how solutions are modeled will be given.

The liquid solution as well as the BCC, Face-Centered Cubic (FCC) or HCP solid solutions can be expressed according to the following equation:

$$G_m^{\varphi} = \sum x_i {}^{\circ}G_m^{\varphi} + RT \sum x_i \ln x_i + {}^{XS}G_m^{\varphi}$$

where ${}^{\circ}G_m^{\varphi}$ corresponds to the Gibbs energy from the linear rule of mixtures regarding the mole fractions x_i of the pure elements i in the phase φ. The second term represents the entropy of mixing for an ideal solution, whereby T is the temperature and R the gas constant. The last term describes the interactions of different elements in a random solution which is usually referred to as excess mixing energy. The excess enthalpy is commonly described in the form of Riedlich-Kister polynomials [34] as follows:

$$
\begin{aligned}
{}^{XS}G_m^{\varphi} = & \sum_i \sum_{j>i} x_i x_j \sum_{\nu=0} {}^{\nu}L_{i,j}^{\varphi} \\
& + \sum\sum\sum \mathrm{x_i x_j x_k}\left[\ {}^{0}L_{i,j}^{\varphi}\left(x_i + \partial_{i,j,k}\right) + \ {}^{1}L_{i,j}^{\varphi}\left(x_j + \partial_{i,j,k}\right) + \ {}^{2}L_{i,j}^{\varphi}\left(x_k + \partial_{i,j,k}\right)\right]
\end{aligned}
$$

where $\partial_{i,j,k}$ is described as $\partial_{i,j,k} = \frac{1-x_i-x_j-x_k}{3}$ and the binary and ternary interaction parameters are represented by $L_{i,j}^{\varphi}\ or\ \ L_{i,j,k}^{\varphi} = a + bT$ with a and b as evaluated model parameters.

To describe intermetallic compounds with certain solubility ranges such as Laves phases or Sigma phases, the sublattice model is a very general model which assigns a sublattice to a distinct crystal lattice site, which correspond to Wyckoff positions in ideal cases. The lattice site can be occupied by multiple atoms and each set of atoms represents a compound the energy of which needs to be described. In this work, for example, the Cr_2Nb or Cr_2Ta Laves phases were modeled by a two-sublattice model. A binary solid solution $[(A,B)_2 : (A,B)]$ can be described by the sublattice model using two lattice sites as follows:

$$
\begin{aligned}
G_m^{\varphi} = & \ y'_A y''_A G^0_{AA} + y'_A y''_B G^0_{AB} + y'_B y''_A G^0_{BA} + y'_B y''_B G^0_{BB} \\
& + RT[2\left(y_A \ln y'_A + y'_B \ln y'_B\right) + \left(y''_A \ln y''_A + y''_B \ln y''_B\right)] \\
& + y'_A y'_B y''_A \sum_{i=0}^{n_1} L_i^1 (y'_A - y'_B)^i + y'_A y'_B y''_B \sum_{i=0}^{n_2} L_i^2 (y'_A - y'_B)^i \\
& + y'_A y''_A y''_B \sum_{i=0}^{n_3} L_i^3 (y''_A - y''_B)^i + y'_B y''_A y''_B \sum_{i=0}^{n_4} L_i^4 (y''_A - y''_B)^i + y'_A y'_B y''_A y''_B L^5
\end{aligned}
$$

where $y'_A,\ y'_B, y''_A$ and y''_B represent the site occupation of the species A or B on the two sublattices marked as inverted commas. The first four terms (so-called end members) describe the contributions of the Gibbs energy reference surface, i.e. phases where each sublattice is occupied by only one type of species: G^0_{AA}, G^0_{AB}, G^0_{BA} and G^0_{BB}. The fifth term refers to the Gibbs energy originating from the contribution of ideal mixing on each sublattice and the remaining terms correspond to the excess Gibbs energy ${}^{XS}G^{\varphi}$.

Thermodynamic database for the Ta-Nb-Mo-Cr-Ti-Al system

Considering the Ta-Nb-Mo-Cr-Ti-Al system, the models used for its pure elements, stoichiometric phases, liquid and solid solutions and intermetallic compounds were briefly described in the previous section. To establish the database for this system consisting of six elements, two elements, i.e. Ta and Nb, were added to the commercial database FRAN acquired by GTT-Technologies[1] which includes the elements Mo, Cr, Ti, Al. The Gibbs energy functions of pure elements were adopted from the open-source SGTE database [35], while thermodynamic data for several stoichiometric phases were taken from the FRAN database (see Tab. 2). Solution phases including intermetallic compounds were modeled using thermodynamic descriptions of binary and ternary systems found in corresponding literature. The phases, their relevant characteristics, the thermodynamic models according to the CALPHAD approach as well as related references used to describe the Ta-Nb-Mo-Cr-Ti-Al system are summarized in Tab. 2.

Table 2: Crystal structure, designation, characteristics and models of phases in the Ta-Nb-Mo-Cr-Ti-Al systems

Phase	Pearson symbol	Space group	Strukturbericht designation	Prototype	Model used in the present description	Reference
L, Liquid					[(Ta, Nb, Mo, Cr, Ti, Al)]	[36–44], FRAN database
α(Al), FCC_A1	cF4	Fm-3m	A1	Cu	$[(Ta, Nb, Mo, Cr, Ti, Al)_1:(Va)_1]$	[36–39,41], FRAN database
α(Ti), HCP_A3	hP2	P63/mmc	A3	Mg	$[(Ta, Nb, Mo, Cr, Ti, Al)_1:(Va)_{0.5}]$	[37,38,41], FRAN database
$\alpha Cr_2Nb/\alpha Cr_2Ta$ (Laves phase)	cF24	Fd-3m	C15	$MgCu_2$	$[(Ta, Nb, Cr, Ti, Al)_2:(Ta, Nb, Cr, Ti, Al)_1]$	[39,43,45], FRAN database
α_2, Ti_3Al	hP8	P63/mmc	D019	Ni_3Sn	$[(Nb, Mo, Ti, Al)_3:(Nb, Mo, Ti, Al)_1]$	[37,39,41]
β, BCC_A2	cI2	Im-3m	A2	W	$[(Ta, Nb, Mo, Cr, Al, Ti)_1:(Va)_3]$	[37,40–43,46] FRAN database
β_0, B2	cI2	Pm-3m	B2	CsCl	$[(Ta, Nb, Mo, Cr, Ti, Al)_{0.5}:(Ta, Nb, Mo, Cr, Ti, Al)_{0.5}(Va)_6]$	[37–39,41,44,47], FRAN database
γ, TiAl	tP4	P4/mmm	L10	AuCu	[(Nb, Mo, Ti, Al):(Nb, Mo, Ti, Al)]	[37,38,41,47]
γ, Cr_2Nb/ Cr_2Ta (Laves phase)	hP12	P63/mmc	C14	$MgZn_2$	$[(Ta, Nb, Cr, Ti, Al)_2:(Ta, Nb, Cr, Ti, Al)]$	[39,43,48], FRAN database
δ, $AlMo_3$	cP8	Pm-3n	A15	Cr_3Si	$[(Nb,Mo,Ti,Al)_3:(Nb,Cr,Al)_1]$	[37], FRAN database
η, $TiAl_2$	tI24	I41/amd	-	$HfGa_2$	$[(Nb, Ti, Al, Ta)_2:(Nb,Ti,Al,Ta)]$	[37,38,47]
ζ, Ti_2Al_5	tP28	P4/mmm		Cu_3Pd	$[(Al, Nb, Ta, Cr,Ti)_2 : (Al, Nb, Ta, Cr,Ti)_5]$	[38,47]
Ti_3Al_5	tP32	P4/mbm	-	Ti_3Al_5	$[(Ti,Nb,Ta)_3:(Al)_5]$	[37,38,47]
ε, $TiAl_3$ (h)	tI8	I4/mmm	D022	$TiAl_3$ (h)	$[(Nb, Mo, Ti, Cr, Al)_{0.75}: (Nb, Mo, Ti, Cr, Al,Ta)_{0.25}$	[36–39,41]

[1] https://gtt-technologies.de/

ε, $TiAl_3$ (l)	tI32	I4/mmm	-	$TiAl_3$(l)	[(Nb, Ta, Mo, Ti, Cr, Al)$_{0.75}$: (Nb, Ta,Mo, Ti, Cr, Al)$_{0.25}$	[37–39]
σ, Nb_2Al	tP30	P42/mnm	D8b	σCrFe	[(Ta, Nb, Mo, Cr, Ti, Al)$_{0.533}$:(Ta, Nb, Ti)$_{0.134}$:(Ta, Nb, Mo, Cr, Ti, Al)$_{0.333}$]	[36–38]
τ, Ti_4NbAl_3	hP6	P63/mmc	B82	Ni_2In	[(Al)$_3$(Nb)$_1$(Ti)$_4$)]	[37,49]
O1 (h) Ti_2NbAl	oC16	Cmcm	-	NaHg	[(Al,Nb,Ta,Ti)$_{0.75}$:(Al,Nb,Ta,Ti)$_{0.25}$]	[37,38,49]
O2 (r) Ti_2NbAl	oC16	Cmcm	-	NaHg	[(Al,Nb,Ti)$_{0.50}$:(Al,Nb,Ti)$_{0.25}$:(Al,Nb,Ti)$_{0.25}$]	[37,49]
$TiAl_2$	oS12	Cmmm		$ZrGa_2$	[($TiAl_2$)]	[47]
Ti_8Al_{17}					[(Ti_8Al_{17})]	FRAN database
$CrAl_4$	*hP*574	P63/mmc		$Mn_{55}Al_{226.58}$	[($CrAl_4$)]	FRAN database
Cr_2Al	tI6	I 4/m m m		$AlCr_2$-$MoSi_2$	[(Cr_2Al)]	FRAN database
Cr_2Al_{11}	*mS**	C1 2/c 1			[(Cr_2Al_{11})]	FRAN database
Cr_2Al_{13}	*mS*104	C12/m1		$Al_{45}V_7$	[(Cr_2Al_{13})]	FRAN database
Cr_4Al_9	*hR**			Cr_4Al_9	[(Cr_4Al_9)]	FRAN database
Cr_5Al_8(s1)	hR26	R 3 m R			[(Cr_5Al_8(s1))]	FRAN database
Cr_5Al_8(s2)	*cI*52	I-43m		Cu_5Zn_8	[(Cr_5Al_8(s2))]	FRAN database
$MoAl_4$	mS30	C1m1		Al_4Mo	[($MoAl_4$)]	FRAN database
$MoAl_5$	hP60	P3		$MoAl_5$	[($MoAl_5$)]	FRAN database
$MoAl_{12}$	CI26	Im-3		$Al_{12}W$	[($MoAl_{12}$)]	FRAN database
Mo_3Al_8	mS22	C12/m1		Mo_3Al_8	[(Mo_3Al_8)]	FRAN database
$Mo_{37}Al_{63}$					[($Mo_{37}Al_{63}$)]	FRAN database
$MoCr_2$					[($MoCr_2$)]	FRAN database
$NbAl_4$					[($NbAl_4$)]	FRAN database
$NbAl_5$					[($NbAl_5$)]	FRAN database
$NbAl_{12}$					[($NbAl_{12}$)]	FRAN database
Nb_3Al_7					[(Nb_3Al_7)]	FRAN database
$Nb_{23}Al_{77}$					[($Nb_{23}Al_{77}$)]	FRAN database

162

3. Results

3.1 Thermodynamic calculations

To understand the nature of the intermetallic and ordered phases formed in the RHEAs NbMoCrTiAl and TaMoCrTiAl, thermodynamic calculations using the commercial software FactSage were performed. The calculations were carried out using the self-developed database including elements Nb, Ta, Mo, Cr, Ti, Al (for details see Tab. 2). In Fig. 1, the phases stable in the alloys NbMoCrTiAl (Fig. 1 (a)) and TaMoCrTiAl (Fig. 1 (b)) between 700 and 1500°C are presented.

According to results of the thermodynamic calculations, the alloys NbMoCrTiAl and TaMoCrTiAl form a single-phase A2 microstructure above 1300 and 1400°C, respectively. At lower temperatures, however, complex intermetallic phases are observed as well. According to the calculations, the Laves phase (C15-type) is a stable phase in both alloys NbMoCrTiAl and TaMoCrTiAl, whereby the solvus temperature of this phase is clearly higher in TaMoCrTiAl. On the contrary, the A15 phase is only stable in the NbMoCrTiAl alloy and exhibits a solvus temperature of about 1200°C. At 1060°C, an A2-to-B2 second order phase transformation was found in both alloys NbMoCrTiAl and TaMoCrTiAl (see Figs. 1 (a) and (b)).

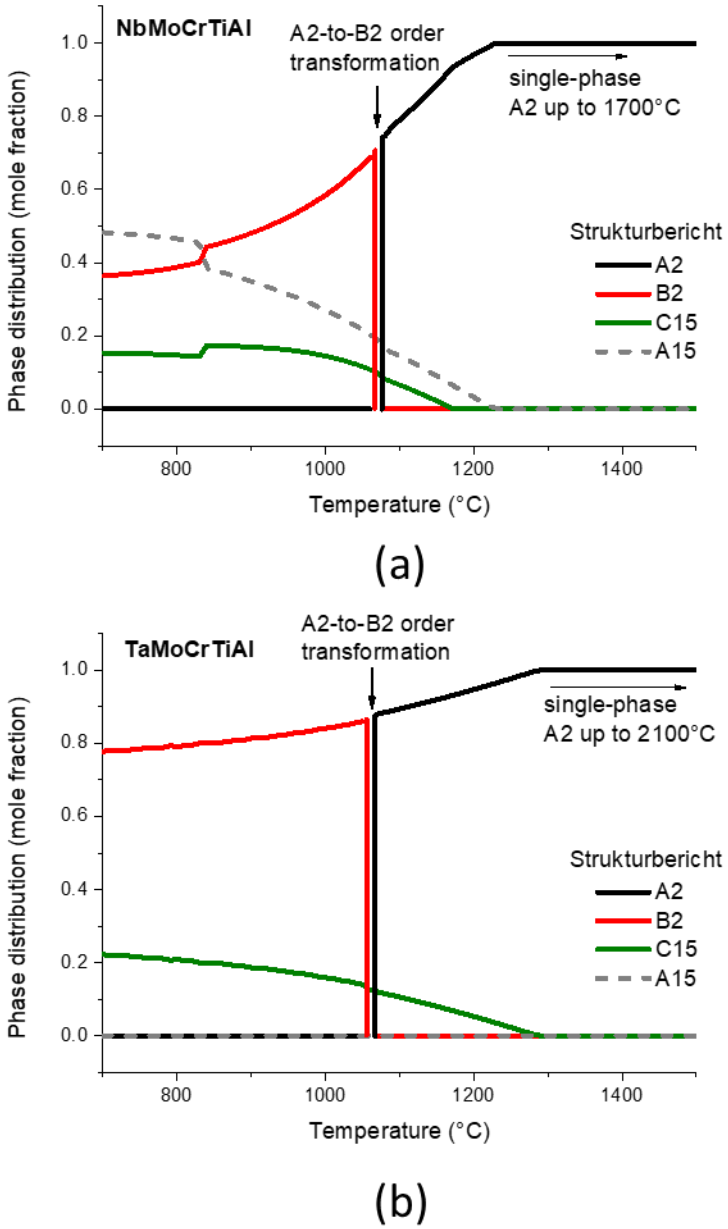

Fig. 1: Calculated equilibrium phase fractions as a function of temperature for (a) NbMoCrTiAl and (b) TaMoCrTiAl. The calculations were carried out using the developed thermodynamic database (Tab. 2) in temperature steps of 10K at a pressure of 1 atm.

3.2. Experimental validation

Detailed microstructural analyses using different techniques were performed (i) to experimentally characterize the alloys studied and (ii) to validate the results of the thermodynamic calculations. The results for the alloys NbMoCrTiAl and TaMoCrTiAl will be presented separately.

NbMoCrTiAl alloy

To identify the crystal structure of the phases in the equiatomic alloy NbMoCrTiAl after annealing, XRD measurements were performed. The XRD analysis of the alloy in the initial condition (annealing at 1300°C for 20h and cooling in the furnace) reveals Bragg peaks that can be assigned to the BCC/A2

(W prototype) phase along with a gentle indication of an ordered B2 (CsCl prototype) crystal structure (see Fig. 2 (a)). No indications of any further phases were observed applying XRD. After annealing at 700°C for 800h, the results of the XRD measurement (Fig. 2 (b)) reveal one additional peak that is accounted for the Cr_2Nb Laves phase (C14, hexagonal). Furthermore, the (100) B2 peak disappears. Increasing annealing temperature up to 800°C results in the formation of an A15-$(Mo,Nb)_3Al$ phase and two Laves phase polytypes (cubic C15 and hexagonal C14) after 300h of exposure (Fig. 2 (c)). The same phases were identified after the annealing treatment at 1000°C for 100h. The metastable hexagonal C36-Cr_2Nb polytype was not found in NbMoCrTiAl in any annealing condition.

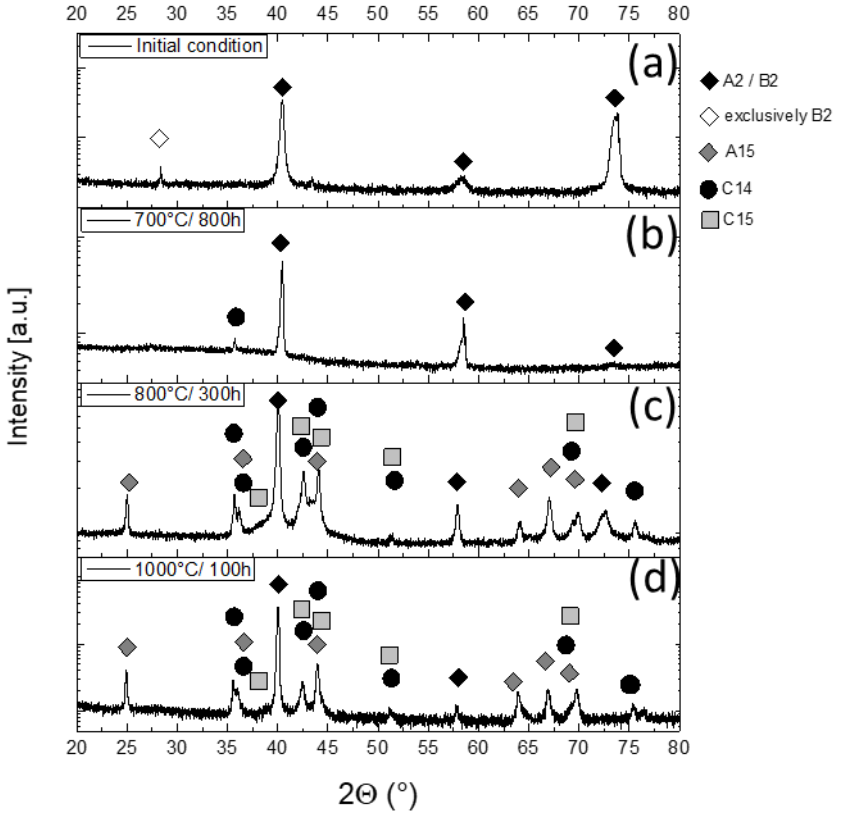

Fig. 2: XRD patterns of NbMoCrTiAl after various annealing conditions: (a) initial condition, (b) 700°C / 800h, (c) 800°C / 300h and (d) 1000°C / 100h

To characterize the microstructures after the different heat treatments, SEM analysis was performed. In the initial condition, the alloy NbMoCrTiAl exhibits an almost single-phase microstructure (see Fig. 3 (a)). Only a small amount of the Cr_2Nb Laves phase (appears as a dark phase) and $Al(Mo,Nb)_3$ A15 phase (appears as a bright phase) can be observed at the grain boundaries. Obviously, these phases were not detected by XRD (see Fig. 2 (a)) because of their small volume fraction << 1 vol.%. The microstructure after heat treatment at 700°C for 800h (Fig. 3 (b)) resembles the appearance of the initial microstructure described above. The volume fraction of the A15 phase did not change significantly, while the volume fraction of the Laves phase seems to increase slightly because this phase was detected by XRD (see Fig. 2 (b)). After annealing at 800°C for 300h, the formation of the Cr_2Nb-Laves phase and the A15 phase seems to intensify as seen by numerous precipitates; especially spherical A15 particles are visible at the grain boundaries as well as in the grain interiors (see Fig. 3 (c)). These observations are in accordance with the XRD results (see Fig. 2 (c)). The microstructure after heat treatment at 1000°C for 100h changes significantly (see Fig. 3 (d)). Firstly, NbMoCrTiAl shows a very fine microstructure. Secondly, the bright phase, presumably A15, forms needle-like precipitates that are

located close to each other. Thirdly, the matrix of the alloy in this annealing condition reveals frequently dark contrast, which is hardly distinguishable due to the comparably fine microstructure. To identify the phases formed in NbMoCrTiAl after annealing at 1000°C for 100h unambiguously, EBSD measurements were carried out.

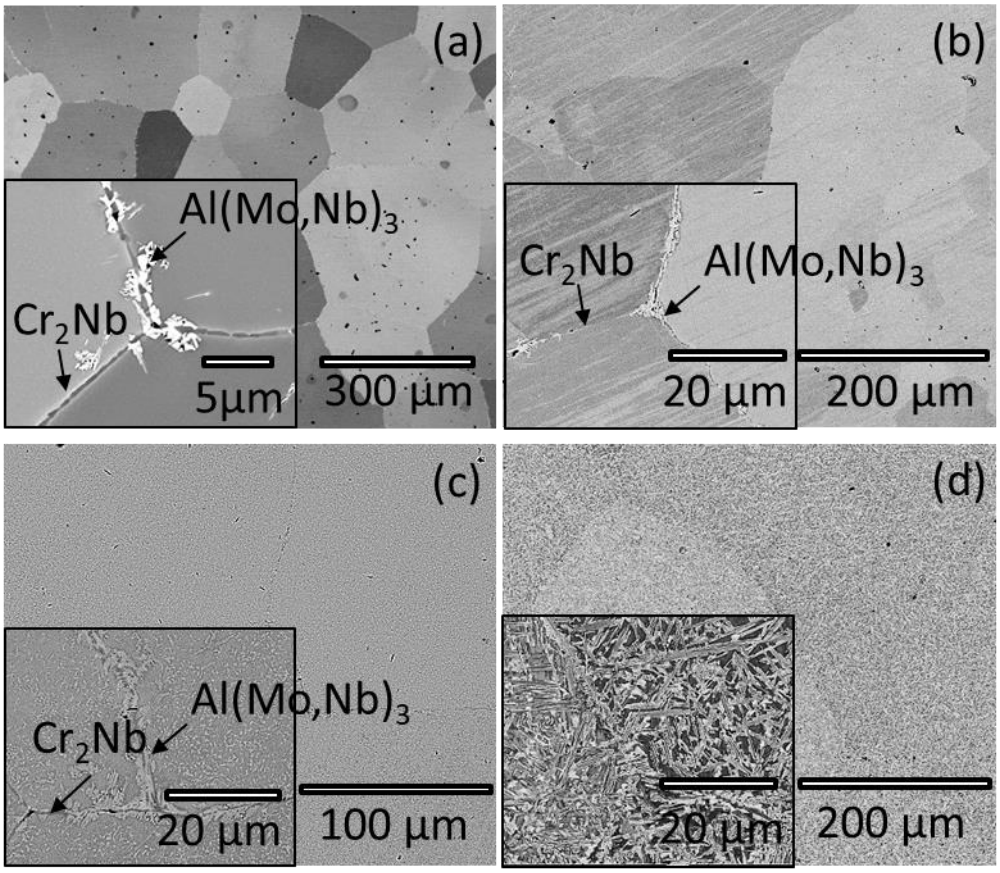

Fig. 3: SEM-BSE images of NbMoCrTiAl: (a) initial condition and after annealing: (b) at 700°C / 800h, (c) at 800°C / 300h, and (d) at 1000°C / 100h. The phase with the bright contrast is $Al(Mo,Nb)_3$, whereas the dark contrast corresponds to Cr_2Nb. The medium greyscale regions depict the B2 matrix phase.

Figure 4 shows results of the EBSD analysis performed on the alloy NbMoCrTiAl after annealing at 1000°C for 100h. A15 and Laves phase precipitates are detected. This result is consistent with the XRD results (compare with Fig. 2 (d)). Further, the A15 area fraction is notably higher (27%) compared to that of the Laves phase (22%).

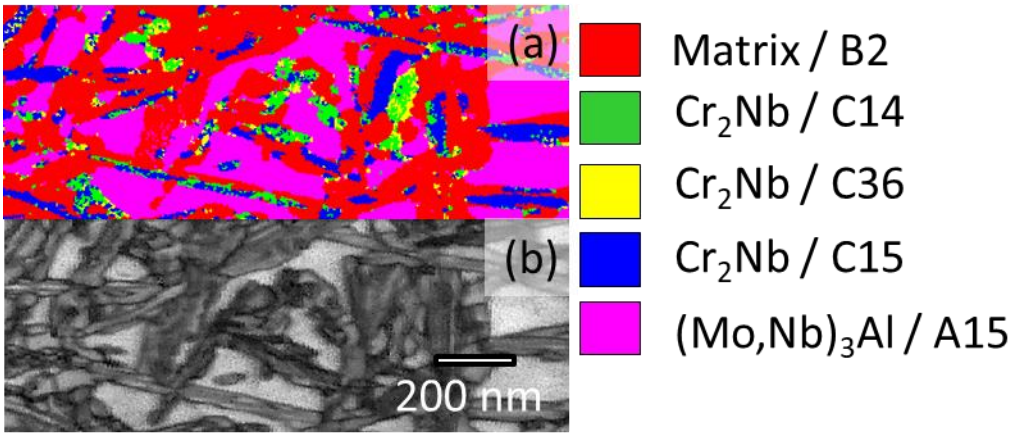

Fig. 4: Results of the EBSD measurements on NbMoCrTiAl after annealing at 1000°C for 100h: (a) phase map according to the color code on the right side and (b) image quality map of the same region in (a).

TaMoCrTiAl alloy

Similar to NbMoCrTiAl, XRD investigations were carried out on the equiatomic alloy TaMoCrTiAl to study the crystal structure of phases formed after various annealing conditions. Figure 5 demonstrates the X-ray diffraction patterns of TaMoCrTiAl in the initial condition (a) and after additional annealing treatments, i.e. at 700°C for 800h (Fig. 5 (b)), at 800°C for 300h (Fig. 5 (c)) and at 1000°C for 100h (Fig. 5 (d)). In all XRD measurements, Bragg peaks of an ordered B2-type (CsCl prototype) crystal structure were found. Furthermore, peaks corresponding to Cr_2Ta Laves phase with hexagonal C14, cubic C15 and dihexagonal C36 polytype were identified. No additional phases could be identified after the annealing treatments. In contrast to the NbMoCrTiAl alloy, no A15 phase was observed in the alloy TaMoCrTiAl.

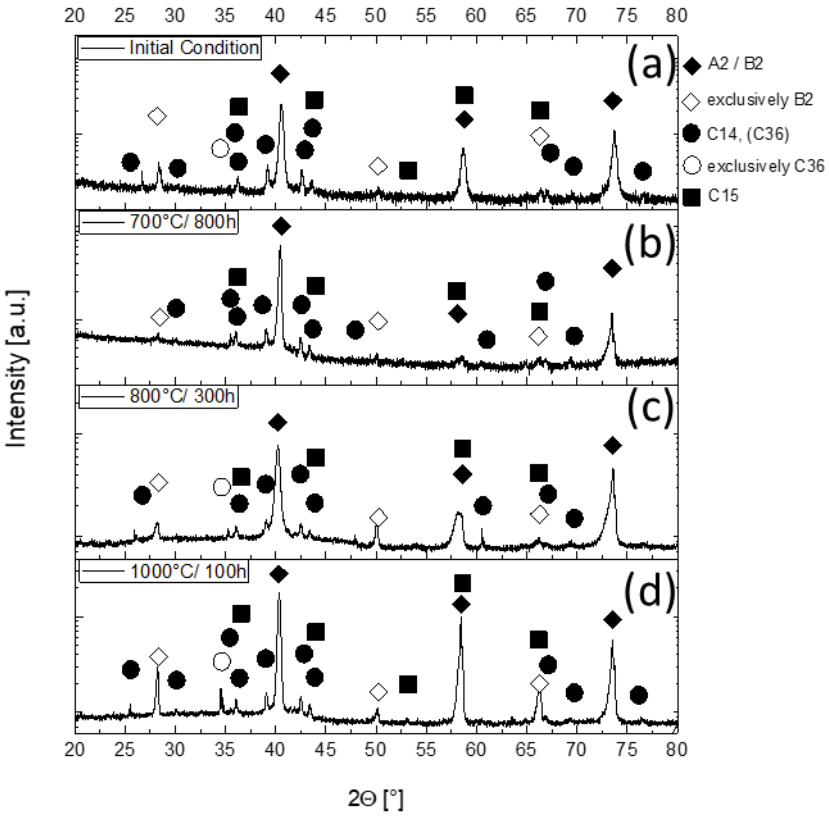

241

242 Fig. 5: XRD patterns of TaMoCrTiAl after various annealing conditions: (a) initial condition,
243 (b) 700°C / 800h, (c) 800°C/300h and (d) 1000°C/100h.

244 In the initial condition, the BSE image illustrated in Fig. 6 (a) shows a matrix phase with large grains of
245 about 100µm and a secondary phase (bright contrast), which forms predominantly at the grain
246 boundaries. According to EDX investigations, EBSD measurements (both are not shown here) and the
247 XRD analysis (Fig. 5 (a)), the secondary phase was identified as Cr_2Ta Laves phase with C14 and C15
248 polytypes. The microstructure after the subsequent annealing at 700°C for 800h (see Fig. 6 (b)) seems
249 to be very similar to the initial condition, i.e. the volume fraction of the Laves phases remains
250 approximately unchanged and no new phases were identified applying XRD (Fig. 5 (c)) and EBSD (not
251 shown here). At higher annealing temperatures, i.e. 800°C for 300h and 1000°C for 100h, the only
252 difference observed is the proceeding of the Laves phase precipitation, also in the grain interior
253 (Fig. 6 (c) and (d)). The presence of the three different forms of Laves phase (C14, C15 and C36) was
254 identified by XRD (Fig. 5 (d)) and verified by EBSD (see Fig. 7).

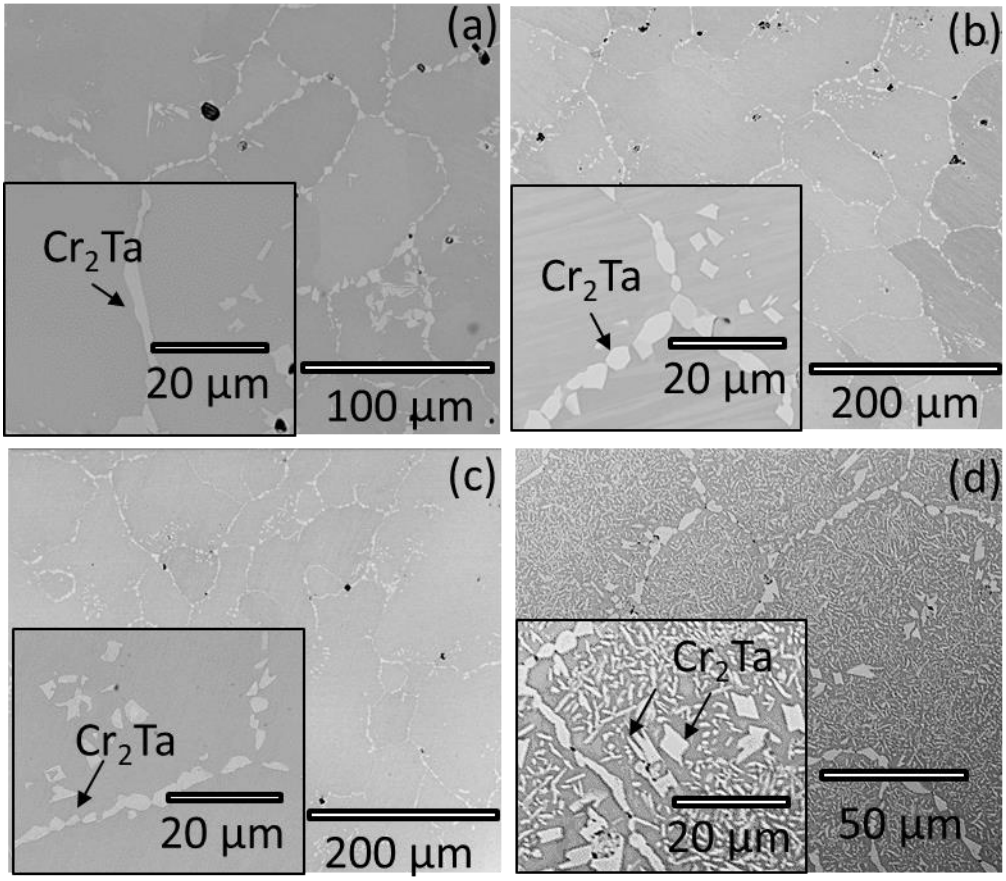

255

256 Fig. 6: SEM-BSE images of TaMoCrTiAl: (a) in the initial condition, (b) after annealing at 700°C /
257 800h, (c) after annealing at 800°C / 300h and (d) after annealing at 1000°C / 100h.

258

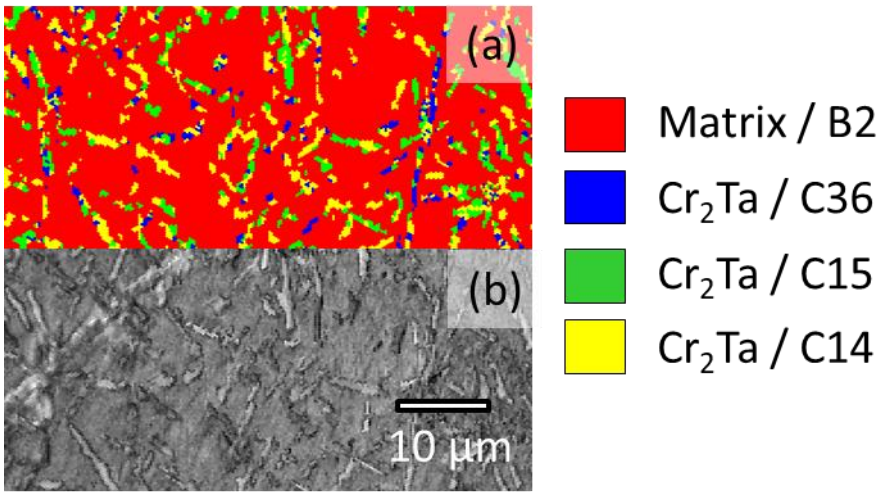

259

260 Fig. 7: Results of the EBSD analysis conducted on the alloy TaMoCrTiAl after annealing at 1000°C
261 for 100h: (a) phase map corresponding to the color code on the right side and (b) image quality of the
262 same region in (a).

263

4. Discussion

Although many studies reported on the single-phase microstructure in HEAs, most of the alloys were investigated after homogenization treatments performed at elevated temperatures followed by a (rapid) cooling [3]. Only selected studies dealt with the phase stability after long-term exposure at intermediate temperatures [50–52]. In terms of potential applications, knowledge about the microstructure in a wide temperature range is however indispensable as the formation of additional, often undesired phases may lead to dramatic failures of technical components. The experimental results shown in this study reveal that the equiatomic alloys NbMoCrTiAl and TaMoCrTiAl are multi-phase materials, each containing several intermetallic equilibrium phases at moderate temperatures. Moreover, the microstructures significantly change during annealing at different temperatures. The chemical nature of the intermetallic phases, in particular, the element partitioning in these phases at various temperatures, will be discussed in this section. Based on this information, conclusions will be drawn allowing a reliable suppression of the complex ordered phases in the RHEAs studied.

A15 Phase:

The formation of some A15 phases, such as $AlNb_3$ or Mo_3Si, should be avoided in HEAs as they are known for their poor mechanical properties, i.e. its high brittleness and high ductile-brittle transition temperature [28,53], as well as their poor oxidation behavior [28,29]. In this work, thermodynamic calculations were used to understand which elements possess a stabilizing effect on the in $AlMo_3$ A15 phase.

The element partitioning in the in $AlMo_3$ A15 phase in different $Nb_xMoCrTiAl$ alloys (with x=0-20 at.% Nb) is illustrated in Fig. 8 (a). The amount of Nb in the A15 phase increases with the increasing nominal Nb content at the expense of Mo while the concentrations of other elements remain unaffected. It can thus be assumed that Nb substitutes Mo in the A15 phase. Indeed, experimental studies on the ternary Nb-Mo-Al system by Hunt et al. [54] reported on the partitioning of Nb on the Mo lattice sites (Wyckoff position 6c) in $Al(Mo,Nb)_3$ A15 phase. Interestingly, no partitioning of Cr into the A15 phase was predicted, which implies that Cr mainly dissolves into the Laves or B2 phase. Further, our calculations reveal an increase of the A15 phase fraction with increasing Nb concentration in the $Nb_xMoCrTiAl$ alloy system (Fig. 8 (b)) which indicates that Nb is a strong stabilizer of the A15 phase.

To conclude, the Nb content should be reduced at least below 10 at.% in order to decrease the A15 phase fraction. If required, a further decrease of the A15 phase fraction can be achieved by a simultaneous reduction in the Mo and Nb concentrations. Further, Ta may serve as an effective substitution for Nb, as no A15 phase was observed in the alloy TaMoCrTiAl.

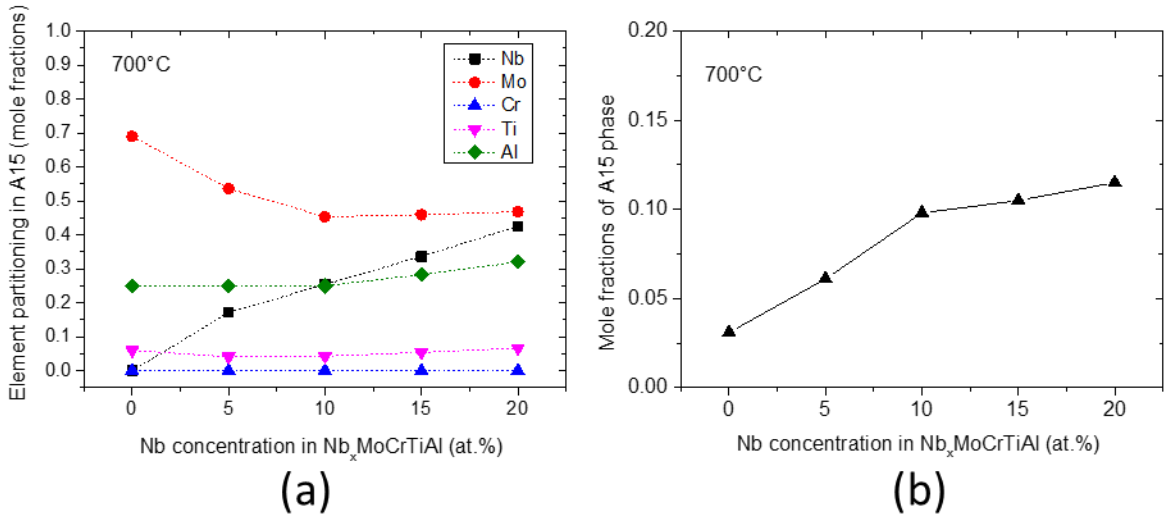

Fig. 8: Effect of different elements on the formation of the A15 phase: (a) element partitioning in the A15 phase in the alloys $Nb_xMoCrTiAl$ with x=0, 5, 10, 15 and 20 at.% at 700°C, (b) mole fractions of the A15 phase dependent on the Nb concentration in the $Nb_xMoCrTiAl$ system at 700°C. Both calculations assume the equimolar ratio between Mo, Cr, Ti and Al.

B2 Phase:

B2-ordered phases may suffer from poor room-temperature ductility mainly due to the inactive <111> slip mode [55–57] or the formation of anti-phase boundaries (APB) if the passage of a single ½ <111> dislocation is active. The poor ductility of the B2 phase was reported for various alloys, e.g. TiAl-based alloys [58], NiAl-based alloys [55] and Al0.5NbTa0.8Ti1.5V0.2Zr [19].

In our previous study, we explored the ordering behavior of the B2 phase and also concluded that the high brittleness of various refractory HEAs from within the Ta-Nb-Mo-Cr-Ti-Al system is most probably attributed by the presence of B2 order [21]. Using differential scanning calorimetry, it was found that an A2-to-B2 disorder-to-order transformation occurs at 1030°C and 1100°C for NbMoCrTiAl and TaMoCrTiAl, respectively [25]. The experimentally determined A2-to-B2 transformation temperatures agree with the calculated temperatures (see Fig. 1).

It is clear that an intrinsic ductile A2-type matrix is mandatory for improving the ductility of the alloys. This can be, for example, achieved by reducing the A2-to-B2 transition temperatures (T_{Trans}^{A2-B2})below potential application temperatures. Here, thermodynamic calculations may be used to understand the constitution of the B2 phase and to reveal possible stabilizing elements of the B2 phase, and to propose new alloy compositions.

The element partitioning in the B2 phase between 700°C and 1000°C was calculated using FactSage and the presented thermodynamic database as depicted in Fig. 9. The results of the thermodynamic calculations show that the Ti and Al concentrations of the B2 phase in both alloys: NbMoCrTiAl (Fig. 9 (a)) and TaMoCrTiAl (Fig. 9 (b)) in the temperature range from 700°C to 1000°C are amongst the highest. Further, the amount of Cr in the B2 phase of NbMoCrTiAl is much higher than in TaMoCrTiAl, while the Mo content is higher in TaMoCrTiAl. The formation of the intermetallic compounds in lower temperatures (compare with Fig. 1), i.e. $Al(Mo, Nb)_3$ A15 phase in NbMoCrTiAl and Cr_2Ta Laves phase TaMoCrTiAl explain the reduction of Nb and Mo (Fig. 9(a)) or Ta and Cr (Fig. 9 (b)) content within the B2 phases with decreasing temperatures.

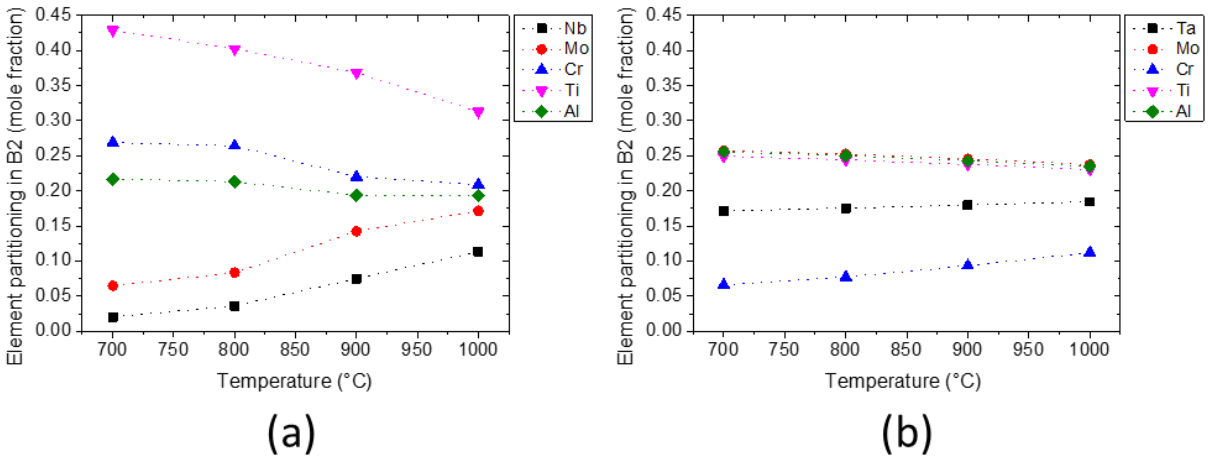

Fig. 9: Element partitioning in the B2 phase within the temperature range 700-1000°C of (a) NbMoCrTiAl and (b) TaMoCrTiAl

Gibbs energies of formation of binary compounds with B2 crystal structure $\Delta G_{i:j}^{B2}$ in the Ta-Nb-Mo-Cr-Ti-Al system were calculated using FactSage and the thermodynamic database presented in Table 2 to evaluate potential stabilizing elements. It has to be noted that the formation energies of $\Delta G_{i:j}^{B2}$ and $\Delta G_{j:i}^{B2}$ are equivalent. Obviously, the Gibbs energies of formation of binary compounds containing Al are amongst the most negatives, i.e. they are the most stable binary compounds with B2 structure in the Ta-Nb-Mo-Cr-Ti-Al system. Especially the compounds Ti:Al, Ta:Al and Nb:Al exhibit the most negative formation energies. In contrast, the Gibbs energies of formation between the residual compounds are either positive or close to zero which implies that the B2 phase of these compounds is meta-stable.

Table 3: Gibbs energies of formation (in kJ/mole) for the B2 phase of binary compounds *i* and *j* ($\Delta G_{i:j}^{B2}$) in the Ta-Nb-Mo-Cr-Ti-Al system assuming a pressure of 1 atm and 273.15K. It has to be noted that $\Delta G_{i:j}^{B2}$ and $\Delta G_{j:i}^{B2}$ are equivalent and thus only values of $\Delta G_{i:j}^{B2}$ are listed below. The calculations were done with FactSage using the self-developed database presented in Table 2.

Element (*i*)	Element (*j*)					
	Ta	Nb	Mo	Cr	Ti	Al
Al	-41.50	-39.47	-28.56	-20.74	-50.72	0
Ti	7.13	5.58	-0.37	10.60	0	
Cr	18.26	24.10	9.82	0		
Mo	-3.30	-3.43	0			
Nb	-3.43	0				
Ta	0					

Further, equilibrium calculations on $TaMoCrTiAl_x$ and $NbMoCrTiAl_x$ (x= 0-20 at.%) (not shown here) indicate that a reduction of Al has a significant effect on the stability of the B2 phase and on the A2-to-B2 transition temperatures. For $TaMoCrTiAl_{10}$, for example, the transition temperature (T_{trans}^{A2-B2}= 700°C), is much lower than for the equimolar TaMoCrTiAl alloy (T_{trans}^{A2-B2}= 1060°C, see Fig. 1 (b)). Also, in $TaMoCrTiAl_{10}$ and $NbMoCrTiAl_{10}$ the thermodynamic calculations reveal the occurrence of an A2/B2 two-phase field at temperatures below 600°C instead of a single B2 phase field like in the equimolar systems (see Figs. 1 (a) and (b). To validate these calculations, however, new alloys with reduced Al concentrations will be investigated in our future works.

Generally, these findings are in accordance with the results of experimental and theoretical studies on B2 phase formation in various related alloy systems. While the occurrence of a B2-type ordering was not reported in many earlier works in the binary Al-Ti system, the results of the DSC measurements of various ternary systems, e.g. Ti-Al-Cr and Ti-Al-Fe [59,60] finally proved its existence [61]. Also, most of the reported RHEAs/CCAs containing Al, Ti, Zr and Nb were found to form an ordered B2 phase [3]. In Al0.5NbTa0.8Ti1.5V0.2Zr [19,20], the chemical composition of the B2 phase was studied by Atom Probe Tomography (APT) yielding clear enrichments in Al, Ti and Zr. As Ti and Zr belong to the same chemical group and might behave similarly, it was concluded that the B2 ordering is likely due to the strong interaction between Al and Ti or Zr [19,20].

Based on the experimental investigations reported in the literature as well as the thermodynamic calculations presented in this study, it can be suggested that primary a reduction of Al concentrations in the Ta-Nb-Mo-Cr-Ti-Al alloy system is effective to reduce the A2-to-B2 transition temperature and (possibly) improve the low-temperature ductility of the alloys studied.

Laves phase:

It is well-known that Laves phases are inherently brittle at room temperature and their formation may also reduce the ductility of the alloys. In our previous works, we reported on the extended formation of the Cr_2Nb and Cr_2Ta Laves phases [22,62] predominantly at the grain boundaries in NbMoCrTiAl and TaMoCrTiAl, respectively. Alloys exhibiting such microstructural peculiarities are usually prone to intercrystalline fracture in case of mechanical loading. To avoid such failure mode, the fractions of Laves phase forming elements, e.g. Ta, Nb and Cr have to be reduced. Thermodynamic calculations provide the required information about the critical concentrations of these elements needed to stabilize or rather destabilize the Laves phase.

Though, three modifications of the Laves phase are known, i.e. the high-temperature hexagonal C14-, the low-temperature cubic C15- and the metastable dihexagonal C36-type. There is some uncertainty about the stability of these modification in particular systems [63–70]. Recent results revealed that the C14 and C36 phases are not stable in the binary Cr-Nb system after annealing [45,67,69,71] but only form as metastable phases in as-cast alloys [69] or in higher-order systems. In the Cr-Ta system, however, few studies report on the low-temperature C15 and the high-temperature C14 form [43,72].

In the two alloys discussed in this work, all three modifications were experimentally identified. The thermodynamic calculations shown in Fig. 10 suggest for both alloys NbMoCrTiAl and TaMoCrTiAl, in the contrary, the formation of the only C15-type Laves phase in the relevant temperature range. Probably, the C14- and C36-type Laves phases appear as metastable stable phases in the alloy systems and require prolonged annealing times to transform into the stable C15-type modification.

It is apparent that to decrease the volume fraction of the Laves phase effectively or even suppress its formation completely, the Cr concentration should be reduced. In Figs. 10 (a) and (b), the phase fractions of Cr_2Nb and Cr_2Ta (both C15-type) are shown in dependence of the nominal Cr concentration at 700°C. According to the equilibrium calculations, the Laves phase starts to form always if Cr (even few at.%) is added to the alloy system NbMoCrTiAl, while Cr concentrations higher than 5 at.% are required for the formation of the Laves phase in the alloy system TaMoCrTiAl. Additional calculations (not shown here) reveal that the reduction of Ta and Nb concentration (in addition to Cr) may further decrease the amount of the Laves phase.

To conclude, the concentrations of Cr and/or Ta/Nb should be reduced to suppress the formation of the Laves phase efficiently. It should, however, be kept in mind that these elements play a crucial role in terms high-temperature strength and high-temperature oxidation resistance [24,73,74].

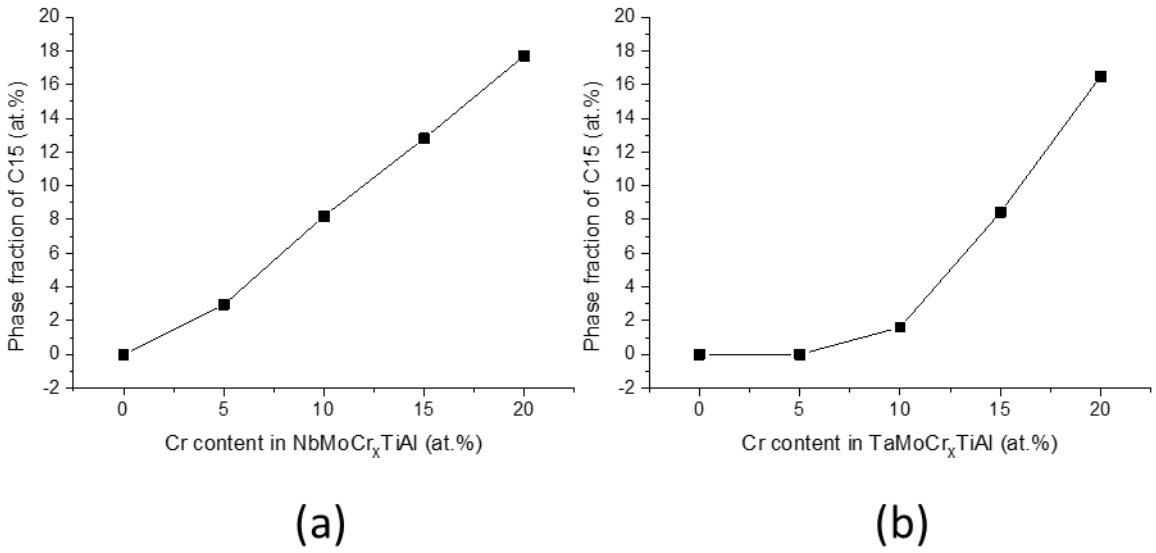

Fig. 10: Effect of Cr on the stability of the Laves phase at 700°C: (a) phase fraction of C15-Cr_2Nb in NbMoCrTiAl, (b) C15-Cr_2Ta in TaMoCrTiAl. Equimolar concentrations of NbMoTiAl and TaMoTiAl were assumed.

4. Conclusion

In this work, a new (self-developed) thermodynamic database was presented. The results of thermodynamic assessments agree well with the experimental observations. From the results of experimental microstructural investigations and thermodynamic calculations, following conclusions can be drawn for the alloy systems NbMoCrTiAl and TaMoCrTiAl:

i) According to the thermodynamic calculations and the experimental observations (presented here and in our previous studies), both quinary alloys NbMoCrTiAl and TaMoCrTiAl form a single-phase BCC/A2 microstructure at sufficiently high temperatures, i.e. 1300°C and 1400°C, respectively.

ii) At intermediate temperatures, intermetallic compounds become thermodynamically stable which have a negative effect of the room-temperature ductility of the alloys. Further, an A2-to-B2 second order transformation at about 1060°C was calculated for both alloys. In case of NbMoCrTiAl, a multiphase microstructure consisting of B2, $Al(Mo, Nb)_3$ and Cr_2Nb Laves phase (C14- and C15-type) are experimentally identified in the initial condition and after annealing experiments at temperatures between 700°C and 1000°C. In the contrary, precipitates of Cr_2Ta Laves phase in the B2 matrix are observed in TaMoCrTiAl. Three different forms of Laves phases, namely C14, C15 and C36-type are identified by XRD and EBSD.

iii) Thermodynamic calculations show that the $AlMo_3$ A15 phase is stabilized by Nb, which obviously substitutes Mo. Therefore, the A15 phase is observed in the alloy NbMoCrTiAl but not in the alloy TaMoCrTiAl.

iv) The presence of B2-type ordering, which was experimentally observed in both equiatomic alloys, seems to be stabilized by predominantly Al. A reduction of the Al concentration below 15 at.% may be suggested to effectively decrease the A2-to-B2 transition temperature.

v) Thermodynamic assessments yield that the concentrations of Cr and/or Ta/Nb should be reduced to suppress the formation of the brittle Laves phase.

5. Acknowledgement

The financial support by the Deutsche Forschungsgemeinschaft (DFG), grant nos. GO 2283/2-1, GO 2283/4-1, HE 1872/31-1 and HE 1872/34-1 is gratefully acknowledged. Part of this work was performed at the Micro- and Nanoanalytics Facility (MnaF) of the University of Siegen.

6. Reference

[1] O.N. Senkov, G.B. Wilks, D.B. Miracle, C.P. Chuang, P.K. Liaw, Refractory high-entropy alloys, Intermetallics 18 (2010) 1758–1765.

[2] O.N. Senkov, G.B. Wilks, J.M. Scott, D.B. Miracle, Mechanical properties of Nb25Mo25Ta25W25 and V20Nb20Mo20Ta20W20 refractory high entropy alloys, Intermetallics 19 (2011) 698–706.

[3] O.N. Senkov, D.B. Miracle, K.J. Chaput, J.-P. Couzinie, Development and exploration of refractory high entropy alloys—A review, J. Mater. Res. 33 (2018) 3092–3128.

[4] N.D. Stepanov, N.Y. Yurchenko, D.V. Skibin, M.A. Tikhonovsky, G.A. Salishchev, Structure and mechanical properties of the AlCrxNbTiV (x = 0, 0.5, 1, 1.5) high entropy alloys, Journal of Alloys and Compounds 652 (2015) 266–280.

[5] H. Chen, A. Kauffmann, S. Laube, I.-C. Choi, R. Schwaiger, Y. Huang, K. Lichtenberg, F. Müller, B. Gorr, H.-J. Christ, M. Heilmaier, Contribution of Lattice Distortion to Solid Solution Strengthening in a Series of Refractory High Entropy Alloys, Metall and Mat Trans A 49 (2018) 772–781.

[6] B. Gorr, F. Mueller, H.-J. Christ, T. Mueller, H. Chen, A. Kauffmann, M. Heilmaier, High temperature oxidation behavior of an equimolar refractory metal-based alloy 20Nb 20Mo 20Cr 20Ti 20Al with and without Si addition, Journal of Alloys and Compounds 688 (2016) 468–477.

[7] W.P. Huhn, M. Widom, Prediction of A2 to B2 Phase Transition in the High-Entropy Alloy Mo-Nb-Ta-W, JOM 65 (2013) 1772–1779.

[8] K.-C. Hsieh, C.-F. Yu, W.-T. Hsieh, W.-R. Chiang, J.S. Ku, J.-H. Lai, C.-P. Tu, C.C. Yang, The microstructure and phase equilibrium of new high performance high-entropy alloys, Journal of Alloys and Compounds 483 (2009) 209–212.

[9] O. Senkov, D. Isheim, D. Seidman, A. Pilchak, Development of a Refractory High Entropy Superalloy, Entropy 18 (2016) 102.

[10] A. Manzoni, H. Daoud, R. Völkl, U. Glatzel, N. Wanderka, Phase separation in equiatomic AlCoCrFeNi high-entropy alloy, Ultramicroscopy 132 (2013) 212–215.

[11] M.-R. Chen, S.-J. Lin, J.-W. Yeh, M.-H. Chuang, S.-K. Chen, Y.-S. Huang, Effect of vanadium addition on the microstructure, hardness, and wear resistance of Al0.5CoCrCuFeNi high-entropy alloy, Metall and Mat Trans A 37 (2006) 1363–1369.

[12] J. Chen, P. Niu, Y. Liu, Y. Lu, X. Wang, Y. Peng, J. Liu, Effect of Zr content on microstructure and mechanical properties of AlCoCrFeNi high entropy alloy, Materials & Design 94 (2016) 39–44.

[13] D.B. Miracle, O.N. Senkov, A critical review of high entropy alloys and related concepts, Acta Materialia 122 (2017) 448–511.

[14] J.Y. He, H. Wang, H.L. Huang, X.D. Xu, M.W. Chen, Y. Wu, X.J. Liu, T.G. Nieh, K. An, Z.P. Lu, A precipitation-hardened high-entropy alloy with outstanding tensile properties, Acta Materialia 102 (2016) 187–196.

[15] E.J. Pickering, R. Muñoz-Moreno, H.J. Stone, N.G. Jones, Precipitation in the equiatomic high-entropy alloy CrMnFeCoNi, Scripta Materialia 113 (2016) 106–109.

[16] K.G. Pradeep, C.C. Tasan, M.J. Yao, Y. Deng, H. Springer, D. Raabe, Non-equiatomic high entropy alloys: Approach towards rapid alloy screening and property-oriented design, Materials Science and Engineering: A 648 (2015) 183–192.

[17] E. Gamsjäger, Y. Liu, M. Rester, P. Puschnig, C. Draxl, H. Clemens, G. Dehm, F.D. Fischer, Diffusive and massive phase transformations in Ti–Al–Nb alloys – Modelling and experiments, Intermetallics 38 (2013) 126–138.

[18] J.K. Jensen, B.A. Welk, R.E.A. Williams, J.M. Sosa, D.E. Huber, O.N. Senkov, G.B. Viswanathan, H.L. Fraser, Characterization of the microstructure of the compositionally complex alloy Al 1 Mo 0.5 Nb 1 Ta 0.5 Ti 1 Zr 1, Scripta Materialia 121 (2016) 1–4.

[19] V. Soni, O.N. Senkov, B. Gwalani, D.B. Miracle, R. Banerjee, Microstructural Design for Improving Ductility of An Initially Brittle Refractory High Entropy Alloy, Scientific reports 8 (2018) 8816.

[20] V. Soni, B. Gwalani, O.N. Senkov, B. Viswanathan, T. Alam, D.B. Miracle, R. Banerjee, Phase stability as a function of temperature in a refractory high-entropy alloy, J. Mater. Res. 33 (2018) 3235–3246.

[21] T.M.M. & Materials Society (Ed.), TMS 2018 147th Annual Meeting & Exhibition Supplemental Proceedings, Springer International Publishing, Cham, 2018.

[22] H. Chen, A. Kauffmann, B. Gorr, D. Schliephake, C. Seemüller, J.N. Wagner, H.-J. Christ, M. Heilmaier, Microstructure and mechanical properties at elevated temperatures of a new Al-containing refractory high-entropy alloy Nb-Mo-Cr-Ti-Al, Journal of Alloys and Compounds 661 (2016) 206–215.

[23] B. Gorr, F. Müller, S. Schellert, H.-J. Christ, H. Chen, A. Kauffmann, M. Heilmaier, A new strategy to intrinsically protect refractory metal based alloys at ultra high temperatures, Corrosion Science 166 (2020) 108475.

[24] F. Müller, B. Gorr, H.-J. Christ, J. Müller, B. Butz, H. Chen, A. Kauffmann, M. Heilmaier, On the oxidation mechanism of refractory high entropy alloys, Corrosion Science 159 (2019) 108161.

[25] H. Chen, A. Kauffmann, S. Seils, T. Boll, C.H. Liebscher, I. Harding, K.S. Kumar, D.V. Szabó, S. Schlabach, S. Kauffmann-Weiss, F. Müller, B. Gorr, H.-J. Christ, M. Heilmaier,

Crystallographic ordering in a series of Al-containing refractory high entropy alloys Ta–Nb–Mo–Cr–Ti–Al, Acta Materialia 176 (2019) 123–133.

[26] S. Laube, H. Chen, A. Kauffmann, S. Schellert, F. Müller, B. Gorr, J. Müller, B. Butz, H.-J. Christ, M. Heilmaier, Controlling crystallographic ordering in Mo–Cr–Ti–Al high entropy alloys to enhance ductility, Journal of Alloys and Compounds 823 (2020) 153805.

[27] K. Li, S. Li, Y. Xue, H. Fu, Microstructure characterization and mechanical properties of a Laves-phase alloy based on Cr2Nb, International Journal of Refractory Metals and Hard Materials 36 (2013) 154–161.

[28] D.M. Shah, D.L. Anton, Evaluation of refractory intermetallics with A15 structure for high temperature structural applications, Materials Science and Engineering: A 153 (1992) 402–409.

[29] J. Zhou, M. Taylor, G.A. Melinte, A.J. Shahani, C.C. Dharmawardhana, H. Heinz, P.W. Voorhees, J.H. Perepezko, K. Bustillo, P. Ercius, J. Miao, Quantitative characterization of high temperature oxidation using electron tomography and energy-dispersive X-ray spectroscopy, Scientific reports 8 (2018) 10239.

[30] K.-Y. Tsai, M.-H. Tsai, J.-W. Yeh, Sluggish diffusion in Co–Cr–Fe–Mn–Ni high-entropy alloys, Acta Materialia 61 (2013) 4887–4897.

[31] O.N. Senkov, J.D. Miller, D.B. Miracle, C. Woodward, Accelerated exploration of multi-principal element alloys with solid solution phases, Nature communications 6 (2015) 6529.

[32] K. Guruvidyathri, K.C. Hari Kumar, J.W. Yeh, B.S. Murty, Topologically Close-packed Phase Formation in High Entropy Alloys: A Review of Calphad and Experimental Results, JOM 69 (2017) 2113–2124.

[33] H.L. Lukas, S.G. Fries, B. Sundman, Computational thermodynamics: The CALPHAD method, Cambridge University Press, Cambridge, 2007.

[34] M. Hillert, Partial Gibbs energies from Redlich-Kister polynomials, Thermochimica Acta 129 (1988) 71–75.

[35] A.T. Dinsdale, SGTE data for pure elements, Calphad 15 (1991) 317–425.

[36] V.T. Witusiewicz, A.A. Bondar, U. Hecht, J. Zollinger, V.M. Petyukh, O.S. Fomichov, V.M. Voblikov, S. Rex, Experimental study and thermodynamic re-assessment of the binary Al–Ta system, Intermetallics 18 (2010) 92–106.

[37] V.T. Witusiewicz, A.A. Bondar, U. Hecht, T.Y. Velikanova, The Al–B–Nb–Ti system, Journal of Alloys and Compounds 472 (2009) 133–161.

[38] V.T. Witusiewicz, A.A. Bondar, U. Hecht, V.M. Voblikov, O.S. Fomichov, V.M. Petyukh, S. Rex, Experimental study and thermodynamic modelling of the ternary Al–Ta–Ti system, Intermetallics 19 (2011) 234–259.

[39] V.T. Witusiewicz, A.A. Bondar, U. Hecht, T.Y. Velikanova, Thermodynamic re-modelling of the ternary Al–Cr–Ti system with refined Al–Cr description, Journal of Alloys and Compounds 644 (2015) 939–958.

[40] J.Y. Lee, J.H. Kim, H.M. Lee, Effect of Mo and Nb on the phase equilibrium of the Ti–Cr–V ternary system in the non-burning β-Ti alloy region, Journal of Alloys and Compounds 297 (2000) 231–239.

[41] N. Saunders, I. Ansara, T. Dinsdale, M.H. Rand, System Ta-Ti, thermo-chemical database for light metal alloys 2 (1997) 293–296.

[42] W. Xiong, Y. Du, Y. Liu, B.Y. Huang, H.H. Xu, H.L. Chen, Z. Pan, Thermodynamic assessment of the Mo–Nb–Ta system, Calphad 28 (2004) 133–140.

[43] N. Dupin, I. Ansara, Thermodynamic assessment of the Cr-Ta system, JPE 14 (1993) 451–456.

[44] D.M. Cupid, M.J. Kriegel, O. Fabrichnaya, F. Ebrahimi, H.J. Seifert, Thermodynamic assessment of the Cr–Ti and first assessment of the Al–Cr–Ti systems, Intermetallics 19 (2011) 1222–1235.

[45] C. Schmetterer, A. Khvan, A. Jacob, B. Hallstedt, T. Markus, A New Theoretical Study of the Cr-Nb System, J. Phase Equilib. Diffus. 35 (2014) 434–444.

[46] C. Marker, S.-L. Shang, J.-C. Zhao, Z.-K. Liu, Thermodynamic description of the Ti-Mo-Nb-Ta-Zr system and its implications for phase stability of Ti bio-implant materials, Calphad 61 (2018) 72–84.

[47] V.T. Witusiewicz, A.A. Bondar, U. Hecht, S. Rex, T.Y. Velikanova, The Al–B–Nb–Ti system, Journal of Alloys and Compounds 465 (2008) 64–77.

[48] C. He, F. Stein, Thermodynamic assessment of the Cr–Al–Nb system, IJMR 101 (2010) 1369–1375.

[49] D.M. Cupid, Thermodynamic assessment of the Ti-Al-Nb, Ti-Al-Cr, and Ti-Al-Mo systems. Doctoral thesis, University of Florida, 2009.

[50] G. Laplanche, S. Berglund, C. Reinhart, A. Kostka, F. Fox, E.P. George, Phase stability and kinetics of σ-phase precipitation in CrMnFeCoNi high-entropy alloys, Acta Materialia 161 (2018) 338–351.

[51] J.E. Saal, I.S. Berglund, J.T. Sebastian, P.K. Liaw, G.B. Olson, Equilibrium high entropy alloy phase stability from experiments and thermodynamic modeling, Scripta Materialia 146 (2018) 5–8.

[52] A. Karati, K. Guruvidyathri, V.S. Hariharan, B.S. Murty, Thermal stability of AlCoFeMnNi high-entropy alloy, Scripta Materialia 162 (2019) 465–467.

[53] A. Misra, J.J. Petrovic, T.E. Mitchell, Microstructures and mechanical properties of a Mo3Si-Mo5Si3 COMPOSITE, Scripta Materialia 40 (1998) 191–196.

[54] C.R. Hunt, A. Raman, Alloy chemistry of sigma (beta)-related phases I. extension of mu- and occurrence of mu-phases in the ternary systems Nb (Ta)--X--Al (X = Fe, Co, Ni, Cu, Cr, Mo), Z. Metallk. 59 (1968) 701–707.

[55] R. Darolia, NiAl alloys for high-temperature structural applications, JOM 43 (1991) 44–49.

[56] R.D. Noebe, R.R. Bowman, M.V. Nathal, Physical and mechanical properties of the B2 compound NiAl, International Materials Reviews 38 (1993) 193–232.

[57] E.P. Lautenschlager, T. Hughes, J.O. Brittain, Slip in hard-sphere CsCl Lmodels, Acta Metallurgica 15 (1967) 1347–1357.

[58] J. Li, B. Song, H. Nurly, P. Xue, S. Wen, Q. Wei, Y. Shi, Microstructure evolution and a new mechanism of B2 phase on room temperature mechanical properties of Ti-47Al-2Cr-2Nb alloy prepared by hot isostatic pressing, Materials Characterization 140 (2018) 64–71.

[59] T.J. Jewett, B. Ahrens, M. Dahms, Stability of TiAl in the TiAlCr system, Materials Science and Engineering: A 225 (1997) 29–37.

[60] R. Kainuma, Y. Fujita, H. Mitsui, I. Ohnuma, K. Ishida, Phase equilibria among α (hcp), β (bcc) and γ (L10) phases in Ti–Al base ternary alloys, Intermetallics 8 (2000) 855–867.

[61] I. Ohnuma, Y. Fujita, H. Mitsui, K. Ishikawa, R. Kainuma, K. Ishida, Phase equilibria in the Ti–Al binary system, Acta Materialia 48 (2000) 3113–3123.

[62] F. Müller, B. Gorr, H.-J. Christ, H. Chen, A. Kauffmann, M. Heilmaier, Effect of microalloying with silicon on high temperature oxidation resistance of novel refractory high-entropy alloy Ta-Mo-Cr-Ti-Al, Materials at High Temperatures 35 (2018) 168–176.

[63] V.M. Pan, Polymorphic Transformation in NbCr2, Fiz. Met. Metalloved. 12 (1961) 455–457.

[64] V.M. Pan, Definition of Equilibrium Diagrams for Cr-Nb and NbCr2-Ni3Nb Systems, Dopov. Akad. Nauk Ukr. RSR 4 (1961) 332–334.

[65] K.S. Kumar, P.M. Hazzledine, Polytypic transformations in Laves phases, Intermetallics 12 (2004) 763–770.

[66] X.-w. Nie, Comments on “The absence of a stable hexagonal Laves phase modification (NbCr2) in the Nb–Cr system”, Scripta Materialia 64 (2011) 990–993.

[67] J. Aufrecht, A. Leineweber, A. Senyshyn, E.J. Mittemeijer, The absence of a stable hexagonal Laves phase modification (NbCr2) in the Nb–Cr system, Scripta Materialia 62 (2010) 227–230.

[68] A. Leineweber, J. Aufrecht, A. Senyshyn, E.J. Mittemeijer, Reply to comments on the absence of a stable hexagonal Laves phase modification (NbCr2) in the Nb–Cr system, Scripta Materialia 64 (2011) 994–997.

[69] J. Aufrecht, A. Leineweber, E.J. Mittemeijer, Metastable Hexagonal Modifications of the NbCr 2 Laves Phase as Function of Cooling Rate, MRS Proc. 1128 (2008) 511.

[70] J. Aufrecht, A. Leineweber, V. Duppel, E.J. Mittemeijer, Transformation–dislocation dipoles in Laves phases: A high-resolution transmission electron microscopy analysis, J. Mater. Res. 25 (2010) 1983–1991.

[71] I.I. Kornilov, K.I. Shakhova, P.B. Budberg, N.A. Nedumov, Phase Diagrams in the System TiCr2-NbCr2, Dokl. Akad. Nauk SSSR 149 (1963) 1340–1342.

[72] K.S. Kumar, L. Pang, C.T. Liu, J. Horton, E.A. Kenik, Structural stability of the Laves phase Cr2Ta in a two-phase Cr–Cr2Ta alloy, Acta Materialia 48 (2000) 911–923.

[73] K.-C. Lo, Y.-J. Chang, H. Murakami, J.-W. Yeh, A.-C. Yeh, An oxidation resistant refractory high entropy alloy protected by CrTaO4-based oxide, Scientific reports 9 (2019) 7266.

[74] W. Ren, F. Ouyang, B. Ding, Y. Zhong, J. Yu, Z. Ren, L. Zhou, The influence of CrTaO4 layer on the oxidation behavior of a directionally-solidified nickel-based superalloy at 850–900 °C, Journal of Alloys and Compounds 724 (2017) 565–574.